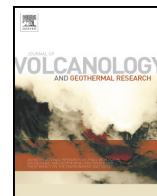




Contents lists available at ScienceDirect

Journal of Volcanology and Geothermal Research

journal homepage: www.elsevier.com/locate/jvolgeores

Quantification of gas and solid emissions during Strombolian explosions using simultaneous sulphur dioxide and infrared camera observations

Talfan Barnie ^{a,*}, Maxime Bombrun ^{a,b}, Michael R. Burton ^c, Andrew Harris ^a, Georgina Sawyer ^a

^a Laboratoire Magmas et Volcans, Université Blaise Pascal, Clermont Ferrand, France

^b Laboratoire d'Informatique, de Modélisation et d'Optimisation des Systèmes, UMR CNRS 6158, Université Blaise Pascal, France

^c Istituto Nazionale di Geofisica e Vulcanologia, Pisa, Italy

ARTICLE INFO

Article history:

Received 3 June 2014

Accepted 2 October 2014

Available online xxxx

Keywords:

Stromboli

Strombolian explosions

Gas imaging

Remote sensing

Sulphur dioxide camera

Thermal camera

ABSTRACT

We present simultaneous measurements of gas and solid emissions from Strombolian explosions acquired on Stromboli volcano on 30 September 2012 using an SO₂ camera and an infrared camera. We find no significant correlation between solid and gas masses, consistent with the postulated independence of the processes controlling bubble film rupture and gas slug mass, which determine emitted solid and gas masses respectively. Our observations demonstrate the utility of simultaneous multi-parametric imaging of volcanic events at different wavelengths to elucidate the relationships between disparate volcanic processes. We also further demonstrate the utility of the SO₂ camera in quantifying explosion dynamics, and that by combining ultra violet camera images and spectral measurements we are able to image the spatial distribution of absorbance by SO₂ in volcanic plumes and, crucially, to calibrate the images to total SO₂ masses while compensating for light dilution effects.

© 2014 Elsevier B.V. All rights reserved.

1. Introduction

Stromboli is the northernmost volcano in the Italian Aeolian Islands volcanic arc, at the boundary of the converging African and European plates (Barberi et al., 1974). Known as the 'lighthouse of the Mediterranean' for its persistent activity—historically documented back to 1000 AD (Rosi et al., 2000)—Stromboli exhibits a range of eruptive behaviour from continuous passive degassing (Allard et al., 1994) through puffing every few seconds (Ripepe et al., 2002), explosions every few tens of minutes (Patrick et al., 2007), major explosions every few months (Aiuppa et al., 2011) up to large Vulcanian paroxysms every few years (Calvari et al., 2006; Aiuppa et al., 2010).

The volcano gives its name to the Strombolian eruption type, characterised by persistent small explosions of around 8 to 17 events per hour (Harris and Ripepe, 2007). These explosions are thought to occur when large over-pressurised gas slugs arrive at the top of the magma column and burst. Gas compositions of the explosion gas and petrological studies of ejected solid material indicate that the slugs are generated at ~3 km depth and rise rapidly to the surface (Burton et al., 2007a; Métrich et al., 2010). Strombolian explosions at the surface consist of two stages; an initial high velocity gas thrust phase determined by the initial maximum velocity at which material is ejected by the bursting bubble, followed by a phase of convective upwelling as the plume entrains surrounding air, cools and rises buoyantly

(Blackburn et al., 1976). The explosions eject both gasses and solids, with the solid component taking the form of bombs that follow ballistic trajectories or fine ash that rises buoyantly with the plume (Patrick et al., 2007). High speed imaging of ballistic events reveals an initial very high speed spray of fine particles (Harris et al., 2012), followed by slower, larger bombs. Multiple pulses of material may be present in a single explosion, which has been attributed to organ pipe resonance (Chouet et al., 1974) or a train of bubbles arriving at the top of the magma conduit in quick succession (Taddeucci et al., 2012).

The term Strombolian activity is frequently used to describe volcanic eruptions globally (e.g. at Heimaey, Iceland (Blackburn et al., 1976), Parícutin, Mexico (Pioli et al., 2008), White Island, New Zealand (Houghton and Nairn, 1991), amongst others), yet some of the most basic physical parameters of Strombolian activity are still poorly constrained, in particular the total masses of gas and solids ejected during a single event. These parameters are therefore needed to define what we mean by Strombolian activity as a category, and the appropriateness of applying the term to a range of eruptive processes worldwide. In addition, they provide constraints on the amount of magma degassing and its partitioning between quiescent and explosive events, as well as on the behaviour of the plumbing system, on modelling the mechanism that generates the explosion and the dispersal of gas and solids, and on the balance between erupted and degassed magma (Harris et al., 2013). Despite being the type locality for Strombolian eruptions and one of the most comprehensively studied and easily accessible volcanoes, there are only six studies at Stromboli estimating the total solid and gaseous emissions from a single explosion,

* Corresponding author. Tel.: +33 473346895.

E-mail address: T.Barnie@opgc.univ-bpclermont.fr (T. Barnie).

with estimates relying on interpreting time series of photographs (Chouet et al., 1974; Ripepe et al., 1993) modelling acoustic processes (Vergnolle and Brandeis, 1996), modelling seismic processes (Chouet et al., 2003), SO₂ camera studies (Mori and Burton, 2009) and identifying cooling bombs on the volcano flank in thermal images (Harris et al., 2013).

In this study we present new observations of Strombolian eruptions acquired with a novel SO₂ camera system and very high frequency thermal camera during a field campaign on the 30th of September 2012, with the aims of 1) expanding the number of estimates of total SO₂ and solids mass ejected during Strombolian activity 2) simultaneously acquiring both mass estimates for the same events to establish if there is a correlation between expelled gasses and solids and 3) test novel SO₂ and infra-red camera systems and processing techniques.

2. Methods

2.1. Calculating erupted solid masses from particle tracking

We derived the total solid mass ejected during an individual explosion using a particle tracking algorithm applied to time series of thermal images. These are particularly useful for capturing the particles emitted by Strombolian explosions due to the high contrast in thermal emission between the hot particles and cold background, which may be indistinguishable in optical images. However, thermal images do have some disadvantages compared to optical images, for instance lower signal to noise ratios and ‘fuzzy’ target boundaries. Here, thermal images were collected using a Forward Looking Infrared (FLIR), this being a FLIR Systems SC655.

The focal plane array of the FLIR camera is composed of uncooled microbolometers sensitive over 7 to 14 μm. The camera was equipped with the 3.6× magnification lens and acquired 640 × 120 images at 200 frames per second. The focal length was 88.9 mm and the instantaneous field of view was 0.19 mrad. During the field campaign, the thermal camera was set up close to the SO₂ camera and at an average distance from the vent of 293 m. With this camera setup and geometry, particles can be detected down to 5.5 cm in size (Holst, 2000), which blend in and out of an image background of the crater wall cluttered with still hot particles from the last explosion. The main challenge in recovering particle sizes is thus removing the background. Here, we used an algorithm based on a mathematical morphology transformation hybridized with a refinement by thresholding (Bombrun et al., 2014). The particles are first distinguished from the static background (non moving, such as crater features) and varying background (moving, such as clouds, birds). They are then enhanced by a mathematical morphology transformation. Pixel dimensions are computed, the long and short axis are found, and by assuming rotational symmetry about the long axis (i.e. the particles are spherical to prolate) the volume is calculated. The mass is calculated by multiplying the volume with an appropriate density. To define an appropriate density conversion, we defined two patterns from distributions collected at Stromboli between 2008 and 2011 (Gurioli et al., 2013; Gurioli et al., 2014). For the bombs (6.5 cm to 35 cm), we see no real trend with increasing size, but the cluster is fairly tight with a mean and standard deviation of 1.8 ± 0.2 g/cm³. Likewise the lapilli field (<6.5 cm) forms a cluster with a mean and standard deviation of 0.98 ± 0.11 g/cm³. We use these two values for our size-dependent conversion to mass, which gives an error in the final total mass on the order of ± 10%.

2.2. Measuring erupted gas masses using an SO₂ camera

We utilised an SO₂ camera system designed by M.B., which consists of two UV-sensitive cameras, model QSI 620s (www.qsimaging.com) mounted with c-mount quartz lenses (25 mm F/2.8 Universe Optics ultraviolet quartz lens) with 10 nm bandpass filters centred at 310 and 330 nm (Asahi Spectra), and an ultra violet spectrometer (Ocean

Optics USB 2000+) connected by a fibre optic cable (Ocean Optics 2 m, 1000 μm core diameter) to a telescope (Ocean optics 74-UV 10 mm f/2 fused silica) pointing within the field of view of the cameras. Each camera has a field of view of 23 by 17.25°, the telescope 5.7°. The cameras and spectrometer are all run from a portable netbook computer on which the spectra and images are stored. The system relies on the principle that the apparent absorbance between the two image bands varies only with species that exhibit non uniform absorbance across them (Mori and Burton, 2006; Mori and Burton, 2009). The bands are therefore chosen such that SO₂ absorbs strongly in one (310 nm) but not the other (330 nm), while aerosols absorb equally in both, resulting in the apparent absorbance between the two bands varying only with SO₂. The apparent absorbance images can then be calibrated to a physical quantity of SO₂ (e.g. in ppm, or parts per million metres) by imaging gas cells of known concentration or by correlating the image time series with SO₂ ppm from fits to ultraviolet spectra.

The data were processed as follows. A flat field correction was applied to each raw count image by subtracting a dark image and dividing by a clear sky image that approximates a uniformly illuminated scene; this procedure corrects for dark current accumulation during exposure and varying response of the CCD-optical system across the image.

$$image_{\lambda,corr} = \frac{image_{\lambda} - dark_{\lambda}}{sky_{\lambda} - dark_{\lambda}} \quad (1)$$

where $image_{\lambda}$, $dark_{\lambda}$, sky_{λ} and $image_{\lambda,corr}$ are the raw count image, dark image, clear sky and corrected image for a band centred at wavelength λ respectively. The negative log was then taken of the corrected images to give the Apparent Optical Depth (AOD). The AOD images were corrected for a wavelength shift in the band pass of the filters as a function of incidence angle which results in a variation in sensitivity to SO₂ cross the scene, using the technique of Smekens et al., in press. Correction images were calculated by imaging gas cells of known SO₂ concentration that fill the field of view of the lenses to image variation in sensitivity with incidence angle, and taking the inverse to get an image containing a correction factor for each pixel.

$$AOD_{\lambda} = -\log\left(image_{\lambda,corr}\right) \times shift_{\lambda} \quad (2)$$

where $shift_{\lambda}$ is the correction image for the wavelength shift and AOD_{λ} is the apparent optical depth. The images were then co-registered using the phase correlation technique to find the geometric transformation between them (Kuglin and Hines, 1975), adapted to include rotation as well as translation (De Castro and Morandi, 1987). This technique rests upon the principle that the offset between an image and a translated copy results in a phase difference between the Fourier transforms of the images. Taking the inverse Fourier transform of this phase difference gives a phase correlation image with an isolated peak at a location that gives the offset in the x and y directions, with an amplitude that decreases as the two images become increasingly dissimilar (e.g. due to differing lighting, acquisition geometry, imaging wavelength, etc.). However, the technique has been found to be robust with respect to variation in illumination and sensor type (Kuglin and Hines, 1975), making it applicable to images acquired at different wavelengths, as in this case. The images were first high pass filtered and had a Hamming window filter applied to localise the registration peak and reduce edge effects. The Fourier transform of each image is then taken, and the phase difference image was calculated and then inverse transformed to give the phase correlation image, with the translation and image similarity given by the location and magnitude of the maximum value. For a given image pair, one image was rotated in increments sufficient to displace a point on the edge by one pixel and the phase correlation procedure applied in each case. The rotation with the largest registration peak was chosen. This rotation, plus the corresponding translation

Download English Version:

<https://daneshyari.com/en/article/6439870>

Download Persian Version:

<https://daneshyari.com/article/6439870>

[Daneshyari.com](https://daneshyari.com)